ACS OMEGA

http://pubs.acs.org/journal/acsodf

Article

Cytotoxic and Apoptotic Effects of Chemogenic and Biogenic Nano-sulfur on Human Carcinoma Cells: A Comparative Study

Samrat Krishnappa, Chandraprabha M. Naganna,* Hari Krishna Rajan,* Sharath Rajashekarappa, and Harish Basavanthappa Gowdru

Cite This: *ACS Omega* 2021, 6, 32548−32562

Read Online

ACCESS | Metrics & More | Article Recommendations | Supporting Information

ABSTRACT: Two-dimensional nanostructures have gained tremendous interest in the field of biomedical applications and cancer activity in particular. Although sulfur is known for its wide range of biological activities, its potentiality in two-dimensional forms as an antitumor agent is hitherto unexplored. To address the current deficient knowledge on nano-sulfur as an antitumor agent, we report the synthesis of nano-sulfur sheets/particles and their cytotoxic, apoptotic activity against human carcinoma cell lines. *In vitro* cytotoxic effects of biogenic nanosheets (SNP-B) and chemogenic nanoparticles (SNP-C) were assessed against human lung carcinoma (A549), human epidermoid carcinoma (A431), human promyelocytic leukaemia (HL60) and human lung fibroblast (IMR90) cell lines. Cell cycle analysis, apoptotic study, and caspase-3 expression studies were carried out to understand the mechanism of cytotoxic activity of nano-sulfur. The MTT assay indicated a dose-dependent decrease in viability of all the cell lines treated with nano-sulfur, with SNP-B being more toxic compared to SNP-C. The apoptotic study and cell cycle analysis indicated cell cycle arrest followed by apoptosis-induced cell death. The caspase-3 expression study indicated that nano-sulfur induces apoptosis by the activation of caspase through the mitochondrial pathway. Apart from this, a lower cytotoxicity was observed in IMR90 cell lines treated with SNP-B , indicating a higher specificity of synthesized nanosheets towards cancer cells. Taken all together, this work highlights the potentiality of sulfur nanosheets in inducing cytotoxicity and apoptotic activity, and the impact of morphology as a critical determinant on the cytotoxic response on various cell lines.

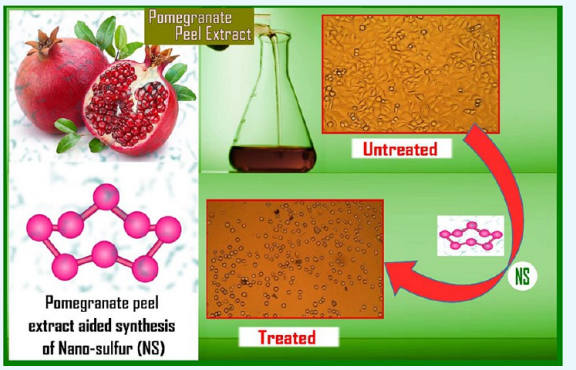

INTRODUCTION

Cancer has become an inexorable threat to public health in recent decades. Among the various types of cancer incidences and mortalities, lung cancer is the most widespread with 2.2 million new cases and 1.8 million deaths in 2020 as per WHO Global Cancer data (GLOBOCAN 2020). India alone accounts for 72,510 new cases and 66,279 deaths.[1,2] The incidence and mortality burden in 2020 of leukemia was reported as 474,519 and 1,198,073, while that of non-melanoma skin cancer was 311,594 and 63,731 (GLOBOCAN 2020). Cancer research has therefore focused on the development of effective anticancer agents that could induce cell death or inhibit the growth of cancer cells. However, the side effects and toxicity associated with poor selectivity have limited the applications of many novel antineoplastic drugs.

The unique physicochemical properties of nanomaterials have facilitated extensive research on the application of nanomaterials in nanomedicine. Numerous metallic and nonmetallic nanomaterials such as silver, gold, titanium dioxide, selenium, iron oxide, silica, and carbon are being explored for cancer therapy and treatment.[3−5] Considering the fact that precious metals such as gold and platinum nanoparticles have been used for various biomedical applications, research on cost-effective strategies to develop novel and cheaper nonmetallic nanomaterials for cancer therapy is an important aspect.

Elemental sulfur, commonly known for its wide range of biological activities, has a long history of being used as one of the ingredients in acne ointments for the treatment of a variety of dermatological disorders like scabies, in antidandruff shampoos, and for acute exposure to radioactive material as an antidote.[6,7] Studies conducted by the Regional Research Institute (Homoeopathy) found that patients treated with sulfur for white patches showed remarkable improvement.[8] Morpholin-4-ium 4-methoxyphenyl (morpholino) phosphinodithioate, a hydrogen sulfide donor, has been reported to exhibit anticancerous activity without affecting normal body

Received: August 2, 2021
Accepted: November 2, 2021
Published: November 23, 2021

ACS Publications

© 2021 The Authors. Published by American Chemical Society

cells.[9] Duan et al. have reported a significant inhibition of the growth of prostate cancer by sulfur treatment.[10] However, the poor solubility, large volume requirement, and huge cost have limited the applicability of sulfur in biomedical field.

Interestingly, different levels of biological activities can be observed with nanoparticles of sulfur (nano-sulfur) when compared to sulfur microparticles. Nano-sulfur, owing to its higher solubility in water at neutral pH, forms sulfides that accelerate the formation of polysulfides that in turn interact with protein sulfhydryl groups and nonprotein molecules, thereby changing their properties.[11] Nano-sulfur has found application as antimicrobial agents, as sulfur-based photocatalysts, in lithium-sulfur batteries, etc.[6,12,13] In spite of extensive interest among researchers, very few reports are available in exploring the potential of nano-sulfur as an antitumor agent. The cytotoxicity and mutagenic activity of nano-sulfur were examined on the L5178Y cell line by Islamov et al.[14] The mechanism of cytotoxic action was assumed to be associated with the interaction of elemental sulfur with sulfhydryl groups of molecules inside the cell. Shankar et al. have examined the cytotoxic effect of nano-sulfur on murine colorectal carcinoma (CT26), Caco-2, human lung carcinoma (A549), and human fibroblast (CCD-986sk) cells.[15] They observed that nano-sulfur could effectively arrest the uncontrolled growth of cancerous cells and inhibit metastasis without being toxic to normal cells.

Various methods have been considered to synthesize nano-sulfur such as liquid phase chemical precipitation,[16] water-in-oil microemulsion,[17] reverse microemulsion using biodegradable iron chelate catalyst from H_2S,[18] and acid-catalyzed precipitation using the aqueous surfactant assisted route.[19] However, all these have disadvantages such as difficulty in the separation and purification of nanoparticles from the microemulsion system, difficulty in the scale-up of the process, and consumption of a large amount of surfactant.[20] Green synthesis of nanoparticles is more advantageous compared to other methods since it is an environmentally benign and faster process that can be carried out at room temperature. Synthesis of nano-sulfur by a green approach has been attempted by few researchers using the extract of plant parts such as *Melia azedarach* leaves,[20] *Albizia julibrissin* fruits,[21] *Acanthophylum bracteatum* stem,[22] *Ficus benghalensis* leaf,[23] *Allium sativum* pulp,[24] *Ocimum gratissimum* leaves,[25] *Rosmarinus officinalis* leaves,[26] *Ocimum basilicum* leaves,[27] *Cinnamomum zeylanicum* bark,[28] *Actinidia deliciosa* fruit peels,[29] etc. However, the biomedical application potential of these nanoparticles is hitherto an unexplored territory. Further, the available literature on the cytotoxic activity of green synthesized nano-sulfur is limited.[15]

The morphology of nanomaterials can have a significant effect on their biological activity. Nanosheets, owing to their unique properties, have been reported to offer several advantages over nanoparticles in biological applications.[30] Kumar et al. in their studies on the cytotoxicity of nanorods and nanosheets of MoS_2 have reported a higher activity of nanorods compared to nanosheets.[31] As far as we know, reports on the comparative analysis of the cytotoxic and antiproliferative properties of nano-sulfur synthesized by different reducing agents or of varying morphologies are unavailable.

In view of this, the present work aims at systematically exploring the cytotoxic effects of nano-sulfur of varying morphologies, synthesized by chemical and biogenic routes, against the human lung carcinoma cell line (A549), human epidermoid carcinoma cell line (A431), human promyelocytic leukaemia (HL60) and human lung fibroblast (IMR90) cell lines. Growth inhibitory effects, apoptotic study, cell cycle analysis, and caspase-3 expression studies have been carried out toward understanding the mechanism of the cytotoxic activity of nano-sulfur.

RESULTS AND DISCUSSION

Synthesis of Chemogenic and Biogenic Nano-sulfur. The present study establishes the rapid synthesis of nano-sulfur using the chemical (SNP-C) as well as biosynthesis method (SNP-B).

Powder X-ray Diffraction (PXRD). To confirm the phase formation and presence of unreacted impurities, powder X-ray diffraction patterns were recorded for sulfur particles prepared by chemical and biological methods and are given in Figure 1a,b respectively. All the observed peaks of SNP-C and SNP-B

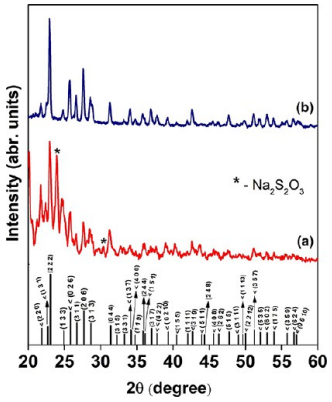

Figure 1. X-ray diffraction patterns of (a) SNP-C (sulfur nanoparticles) and (b) SNP-B (sulfur nanosheets).

are found to be well resolved, and the pattern observed for both the samples readily matches with the S_8 structure of α-sulfur (JCPDS card no. 01-078-1889), which confirms that nano-sulfur is of an orthorhombic phase. It can also be seen from the XRD pattern that the diffraction peaks of SNP-C are relatively less intense than those of the SNP-B. Since the conditions (such as scan rate, amount of sample, sample height, and zero background) of X-ray data collection for both the samples are the same, we can infer that the difference in diffraction peak intensity is due to the difference in the crystallinity of the samples prepared by different methods. To assess the effect of the synthesis method, crystallite size was calculated using Debye−Scherrer's formula and found to be 40 and 37 nm for SNP-C and SNP-B, respectively.[32] The lower crystallite size in case of SNP-B may be due to the phytoconstituents of extract acting as capping agents that control the crystal growth and size.[33] Further, in case of the XRD pattern of SNP-C, the impurity peak was found at 2θ = 24° that can be attributed to the unreacted sodium thiosulfate precursor.[34] However, in SNP-B, no impurity phases are detected in the XRD pattern.

Scanning Electron Microscopy (SEM). Scanning electron micrographs (SEMs) of sulfur prepared by biological and chemical methods are shown in Figure 2a,b and c,d respectively. The surface morphology of SNP-B shows agglomerated sheets with porous structures. Higher-magnifi-

https://doi.org/10.1021/acsomega.1c04047
ACS Omega 2021, 6, 32548−32562

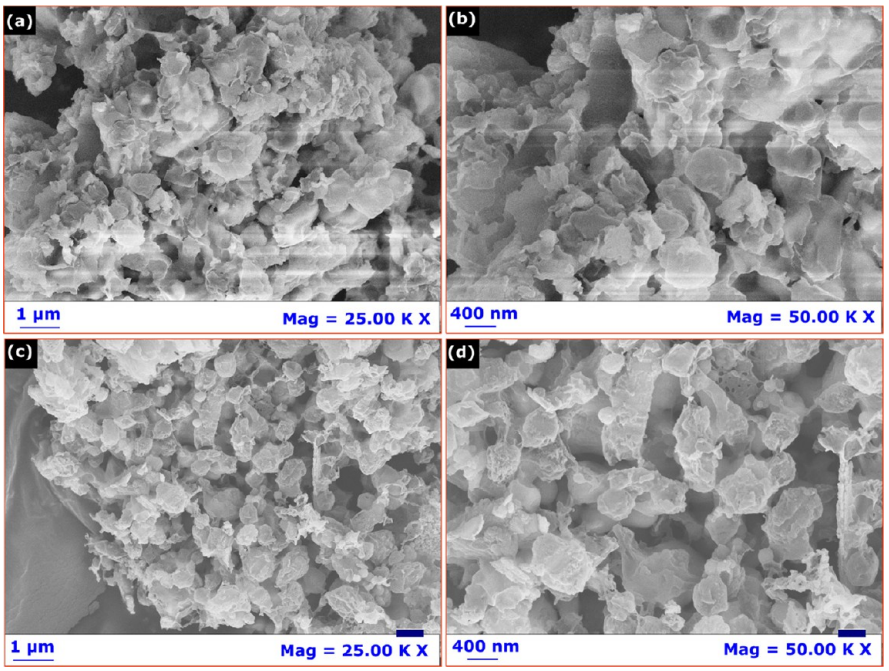

Figure 2. SEM micrograph of SNP-B (a, b) and SNP-C (c, d) at different magnifications.

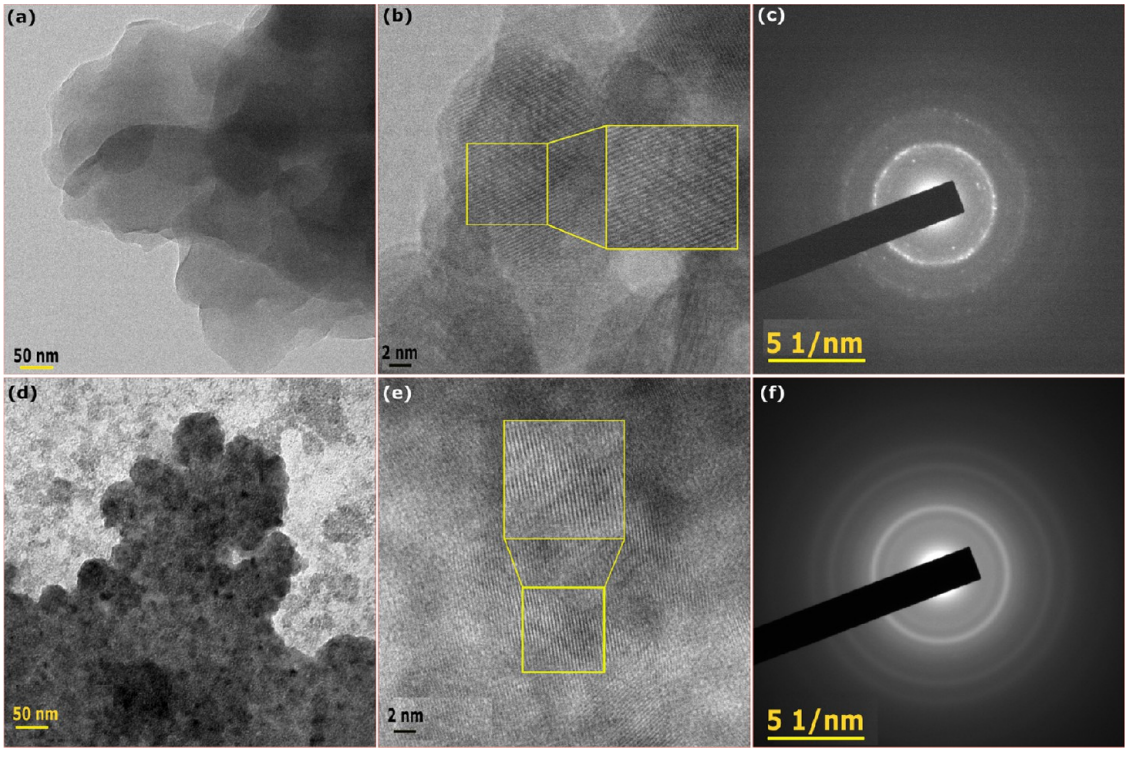

Figure 3. TEM images of (a) SNP-B and (d) SNP-C. HRTEM images of (b) SNP-B and (e) SNP-C. SAED patterns of (c) SNP-B and (f) SNP-C

cation images show that the sulfur sheets have a smooth surface. The sheets formed have different sizes. The reason for the formation of sheetlike structures can be ascribed to the complex composition of the peel extract. The LC−MS data reported by Young et al.[35] and by others[36−38] show that the *Punica granatum* peel extract contains gallic acid and punicalagin as major phenolic compounds, in addition to other phenolic acids such as caffeic acid, granatin A, cyanidin granatin B, quercetin, chlorogenic acid, punicalin, ellagic acid, pelargonidin, and apigenin. On the other hand, the morphology of SNP-C (Figure 2c,d) shows particle agglomerates and the agglomerates form clusters of varying sizes. Further, the surface structure of the SNP-C is also found to be of a porous nature due to the numerous voids and fine pores seen. Unlike SNP-B, the surface morphology of SNP-C is not smooth and shows accumulation of fine particles distributed unevenly, making the surface rough. The particles and the

https://doi.org/10.1021/acsomega.1c04047
ACS Omega 2021, 6, 32548−32562

agglomerates have irregular shape and size and a non-uniform distribution.

Transmission Electron Microscopy (TEM). The transmission electron microscopic images of SNP-B and SNP-C are shown in Figure 3a,b and d,e, respectively. The TEM micrographs of SNP-B have sheetlike structures that resemble the TEM images of graphene with a size range of 10−20 nm. The sheets of sulfur have multiple layers overlapped that can be clearly visible in Figure 3a. However, TEM of SNP-C shows particle agglomerates, and the extent of agglomeration is so high that individual particles could not be differentiated. The average size of the agglomerated clusters is ∼30−40 nm. The agglomerated nature of the particles observed in TEM images of SNP-C is consistent with the SEM results. The HRTEM images (Figure 3 b,e) show well-defined lattice fringes with d-spacings ∼0.32 and 0.38 nm for SNP-B and SNP-C, respectively. These correspond to the (206) and (222) plane of orthorhombic sulfur. Figure 3c,f shows the SAED pattern, and the nature of the diffracted pattern is found to be a ring pattern with spots indicating the nano-crystalline nature of sulfur.[39]

Raman Spectroscopy. To better understand the structural features and phase formation of the products, SNP-C and SNP-B are characterized by Raman spectroscopy and the spectra are presented in Figure 4a,b. Sulfur is found to show a

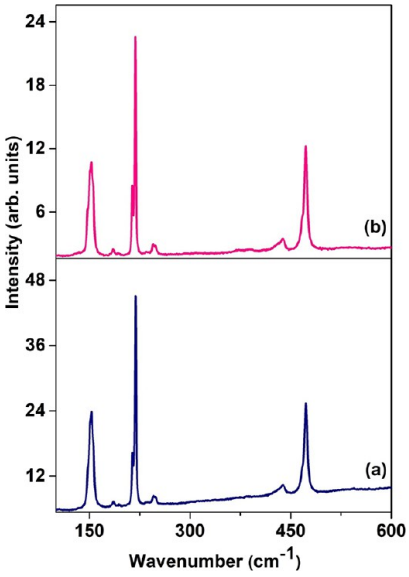

Figure 4. Raman spectra of (a) SNP-B and (b) SNP-C.

decomposition behavior at particular laser excitations. Therefore, in the present study, we have used a 632 nm laser excitation source that is more suitable for sulfur. It can be seen that both the samples (SNP-C and SNP-B) show well-resolved intense peaks at 153, 213, 219, and 473 cm^{-1}. Further, weak peaks at 186, 245, and 438 cm^{-1} are also observed in both the spectra. These peaks are in accurate agreement with the elemental sulfur reported in the literature.[40−43] The Raman modes for sulfur (S8) with a D4d symmetry are $2A_1 + 3E_2 + 2E_3$, and it is as given by Scott et al.[44] The peak at 153 cm^{-1} can be assigned to the E_2 symmetry species, and those peaks at 219 and 473 cm^{-1} are due to the A_1 species. Further, weak peaks at 245 and 438 cm^{-1} can be assigned to the E_3 species, and the peak at 186 cm^{-1} is Raman forbidden, appearing in violation of D4d selection rules.[45]

Cell Viability Assay. An MTT assay was performed to determine the effect of ST, PPE, and nano-sulfur (SNP-C and SNP-B), respectively, on the cell viability of A549, A431, and HL60 cancer cell lines at various concentrations (12.5, 25, 50, 100, and 200 μg/mL). The results showed a decrease in the viability of cells in a concentration-dependent manner for all the cell lines (Table 1 and Figure 5). IC_{50} values of ST and PPE toward A549 cell lines at 24 h were 155.36 ± 2.95 and 232.16 ± 2.47 μg/mL, respectively (Table S1 and Figure S1). For A431 cell lines, the IC_{50} values of ST and PPE were 142.41 ± 1.46 and 209.06 ± 3.48 μg/mL, respectively. In the case of HL60, the IC_{50} values of ST and PPE were 177.11 ± 2.13 and 230.04 ± 3.26 μg/mL, respectively, whereas the IC_{50} values of SNP-B and SNP-C toward A549 cell lines at 24 h were 9.5 ± 0.29 and 129.3 ± 0.23 μg/mL, respectively. For A431 cell lines, the IC_{50} values of SNP-B and SNP-C were 18.29 ± 0.09 and 122.4 ± 1.69 μg/mL, respectively. For HL60, the IC_{50} values of SNP-B and SNP-C were 10.49 ± 0.52 and 153.2 ± 0.19 μg/mL, respectively (Table 1). In contrast, the IC_{50} values of SNP-B and SNP-C for IMR90 cell lines were 443.8 ± 5.11 and 342.7 ± 12.29 μg/mL, respectively (Table 1 and Figure 5). From the cell viability assay, it was observed that both ST and PPE indicated lower cytotoxic effects compared to synthesized nano sulfur (SNP-C and SNP-B). Apart from this, SNP-C is less toxic compared to SNP-B against all the tested cancer cell lines, whereas SNP-B exhibited lower cytotoxic effects than SNP-C against IMR90 cell lines (normal cells). This specificity of sulfur nanoparticles toward cancer cell is clinically important and demonstrates its capacity for being a chemopreventive or therapeutic agent. Also, one of the major challenges of any anticancer drug to be free from any side effects is to effectively distinguish tumor cells from normal cells. Similar results were reported by Shankar et al. wherein dose-dependent lower cytotoxic effects were observed for sodium thiosulfate against CT26 cell lines compared to sulfur nanoparticles at 500 μg/mL, whereas in the case of A549 cell lines, sodium thiosulfate did not show any significant cytotoxic effect at the tested concentration range of 10 to 1000 μg/mL.[15] Sukri et al. reported lower cytotoxic effects and a decrease in cell viability by PPE against colon cancer cell lines (HCT116) at 250 μg/mL.[37] Further, as observed from Figure 5, cell lines treated with a standard drug and nano-sulfur exhibited condensed and floating cells with a significant decrease in cell density compared to the untreated cell lines. Shrinking of cells with blebbing and rupturing of membranes are also observed for nano-sulfur treated cell lines. The cytotoxic effect as indicated by Figure 5 is higher for SNP-B compared to SNP-C. The observed difference in the cytotoxic effect of nano-sulfur could be attributed to the different reducing agents used during synthesis or the altered morphology of SNP-B (nanosheets) and SNP-C (nanoparticles). The present study proves the impact of morphology on the cytotoxicity of nano-sulfur.

Apoptosis Study. The cell viability assay exhibited the dose-dependent cytotoxic effect of the prepared nano-sulfur (SNP-B and SNP-C). However, the mechanism underlying the cell death needs to be understood. The Annexin V−FITC/propidium iodide (PI) dual staining method was used to assess the apoptotic and non-apoptotic population of cells through flow cytometry. In case of cell lines treated with nano-sulfur, the stained cells showed increased cell population percentage along with increased Annexin V uptake in lower and upper right coordinates (Table 2 and Figure 6) and decreased viable cell percentage (Annexin V−/PI−) in the lower left

https://doi.org/10.1021/acsomega.1c04047
ACS Omega 2021, 6, 32548−32562

Table 1. Percentage Cell Viability of A549, A431, HL60 and, IMR90 Cell-Lines Treated with Various Concentrations of SNP-B and SNP-C[a]

	cell viability (%)									
	control	standard	test sample							
test compound	untreated	standard drug	12.5 (μg/mL)	25 (μg/mL)	50 (μg/mL)	100 (μg/mL)	200 (μg/mL)	9.5 (μg/mL)	129.3 (μg/mL)
A549 cell lines									
SNP-B	100 ± 0	51.03 ± 0.10***	48.34 ± 0.08***	32.06 ± 0.21***	21.26 ± 0.38***	12.24 ± 0.39***	2.18 ± 0.47***	-	-
SNP-C			98.34 ± 0.11***	93.2 ± 0.21***	83.36 ± 0.14***	59.91 ± 0.14 ***	21.82 ± 0.19***	-	-
A431 cell lines									
SNP-B	100 ± 0	50.28 ± 0.64***	57.82 ± 0.09***	40.91 ± 0.16***	34.78 ± 0.42***	18.75 ± 0.77***	6.86 ± 0.77***	-	-
SNP-C			94.27 ± 0.69***	88.07 ± 0.30***	74.72 ± 0.39***	55.20 ± 0.46***	22.42 ± 1.01***	-	-
HL60 cell lines									
SNP-B	100 ± 0	46.58 ± 1.84***	49.52 ± 0.60***	38.98 ± 0.55***	29.54 ± 0.62***	22.17 ± 0.39***	16.64 ± 0.64***	-	-
SNP-C			93.81 ± 0.30***	89.68 ± 0.06***	83.63 ± 0.68***	64.44 ± 0.25***	36.08 ± 0.19***	-	-
IMR90 cell lines									
SNP-B	100 ± 0	67.16 ± 0.35***	98.06 ± 0.90	97.12 ± 0.70*	93.26 ± 1.03***	88.26 ± 0.98***	77.24 ± 0.41***	98.99 ± 0.23	-
SNP-C			96.38 ± 0.34*	93.96 ± 0.64***	91.38 ± 0.49***	85.57 ± 1.30***	69.40 ± 0.98***	-	79.90 ± 0.60***

[a]Values are expressed as the mean ± SEM ($n = 3$). Statistical significance (P) calculated by one-way ANOVA followed by Dunnett's test. ***$P < 0.001$, **$P < 0.01$, and *$P < 0.05$ were considered as statistically significant by comparing the treated group with the control group.

coordinate. Early (Annexin V+/PI+) and late (Annexin V +/PI−) apoptotic cell percentages in A549 cell lines treated with IC_{50} SNP-B were 33.11 ± 3.12 and 34.67 ± 2.47%, respectively, while percentages in those treated with IC_{50} SNP-C were 38.83 ± 1.85 and 3.61 ± 0.86%, respectively. Early and late apoptotic cell percentages for A431 cell lines treated with IC_{50} SNP-B were 12.77 ± 1.91 and 32.67 ± 0.93%, respectively, while percentages in those treated with IC_{50} SNP-C were 15.96 ± 2.87 and 15.35 ± 0.87%, respectively. For HL60 cell lines treated with IC_{50} SNP-B, percentages of early and late apoptotic cells were 21.83 ± 3.77 and 21.68 ± 1.36%, respectively, and for those treated with IC_{50} SNP-C, percentages were 13.37 ± 4.07 and 17.91 ± 1.85%, respectively. In contrast, for IMR90 cell lines treated with IC_{50} SNP-B and SNP-C, respectively, early and late apoptotic cells were much less for SNP-B treated (0.06 ± 0.03 and 0.49 ± 0.25%) than SNP-C treated (8.89 ± 3.54 and 1.63 ± 0.50%) cell lines (Table 2 and Figure 6). Necrotic cell percentages (Annexin V−/PI+) in A549, A431, HL60, and IMR90 cell lines treated with nano-sulfur at IC_{50} concentration were 1.09 ± 0.11, 5.59 ± 0.73, 31.08 ± 2.94, and 2.36 ± 0.30% for SNP-B, respectively, whereas in case of SNP-C, percentages were 4.75 ± 1.37, 3.47 ± 0.89, 13.21 ± 1.02, and 1.59 ± 0.29%, respectively. In contrast, early apoptotic, late apoptotic, and necrotic cell percentages in untreated cells were very low (A549: 0.89 ± 0.75, 0.26 ± 0.18, and 0.85 ± 0.49%; A431: 2.19 ± 1.13, 1.25 ± 0.48, and 1.38 ± 0.26%; HL60: 0.97 ± 0.47, 1.09 ± 0.62, and 2.39 ± 0.45%) when compared to nano-sulfur treated cells. The obtained results indicate that nano-sulfur induces early cell apoptosis and late cell apoptosis indicative of apoptotic cell death in all the treated cell lines. However, sulfur nanoparticles exhibited higher apoptotic cell death in A549 cell lines than IMR90 cell lines. SNP-B exhibited higher apoptotic cell death in all the treated cell lines compared to SNP-C, considering both early and late apoptotic cell percentage. Further, HL60 cell lines treated with nano-sulfur exhibited a higher percentage of necrotic cells in comparison with A549 and A431 cell lines. This is because of the fact that it is easy for HL60 cell lines, being suspension cells, to exhibit a higher amount of cell debris that might be due to a higher rate of cellular internalization of nano-sulfur,[46] whereas A549 and A431 cell lines, being adherent cells, express a negligible amount of cell debris.

Cell Cycle Analysis. One of the effective screening assays for potential therapeutic drugs is cell cycle progression. Estimating the cellular DNA content is essential to assess the cell cycle. This was assessed by flow cytometry that allows discrimination between G1, S, G2, and M phases. The starting point for the cell cycle is the gap 1 phase (G1), during which the cell prepares, grows in size, and synthesizes mRNA and proteins required for DNA synthesis. During the synthesis phase (S), the replication of DNA occurs, and in the gap 2 phase (G2), the cell grows some more in size, produces new proteins required, and prepares for cell division. Finally, the cell enters the mitosis phase (M), where the cell divides into two daughter cells and enters the G1 phase. Further, the cells that stop dividing temporarily enter the resting phase called the gap zero phase (G0) and are metabolically active. Therefore, analysis of cell cycle progression was performed by propidium iodide (fluorescent nucleic acid dye) staining, and the results obtained are shown in Table 3 and Figure 7. A significant increase in the percentage of cells arrested in the G2/M phase of cell cycle was observed. It can be noted that, in this phase,

https://doi.org/10.1021/acsomega.1c04047
ACS Omega 2021, 6, 32548−32562

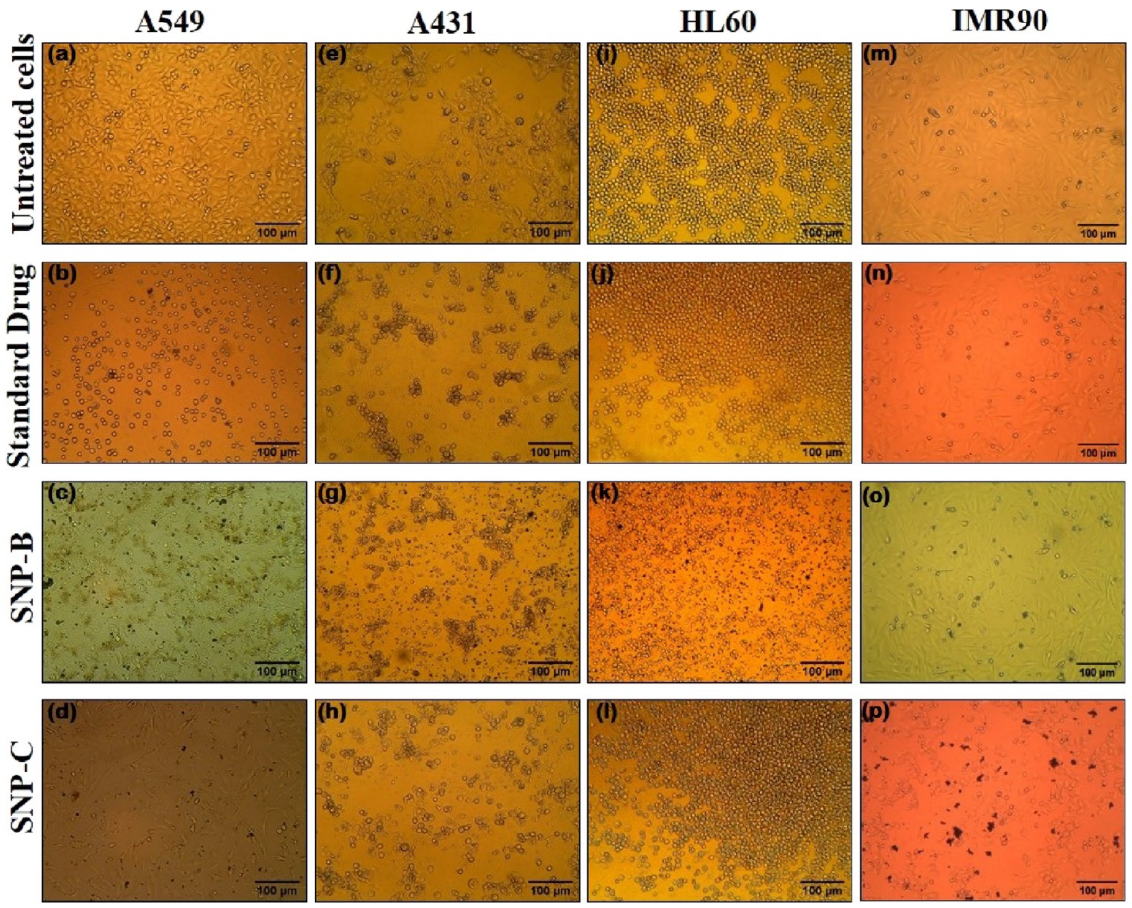

Figure 5. Morphological changes of A549, A431, HL60, and IMR90 cell-lines un-treated (a, e, i, m) and, treated with IC_{50} concentration of the standard drug (b, f, j, n), SNP-B (c, g, k, o), and SNP-C (d, h, l, p) after 24 h treatment.

Table 2. Apoptotic Study (i.e., Annexin V/PI Expression Study) of SNP-B and SNP-C against A549, A431, HL60, and IMR90 Cell-Lines[a]

quadrant	% viable cells	% early apoptotic cells	% late apoptotic cells	% necrotic cells
label	UL	UR	LL	LR
		A549 cell lines		
untreated	98.00 ± 1.11	0.89 ± 0.75	0.26 ± 0.18	0.85 ± 0.49
standard drug	13.58 ± 1.57***	36.85 ± 1.67***	47.39 ± 2.61***	2.18 ± 0.58
SNP-B	31.13 ± 0.80***	33.11 ± 3.12***	34.67 ± 2.47***	1.09 ± 0.11
SNP-C	52.80 ± 1.77***	38.83 ± 1.85***	3.61 ± 0.86	4.75 ± 1.37*
		A431 cell lines		
untreated	95.17 ± 1.53	2.19 ± 1.13	1.25 ± 0.48	1.38 ± 0.26
standard drug	34.06 ± 1.77***	3.77 ± 0.67	38.29 ± 2.75***	23.88 ± 1.74***
SNP-B	48.97 ± 1.27***	12.77 ± 1.91**	32.67 ± 0.93***	5.59 ± 0.73
SNP-C	65.22 ± 1.49***	15.96 ± 2.87**	15.35 ± 0.87***	3.47 ± 0.89
		HL60 cell lines		
untreated	95.55 ± 1.51	0.97 ± 0.47	1.09 ± 0.62	2.39 ± 0.45
standard drug	65.73 ± 1.18***	18.13 ± 1.52**	6.18 ± 0.58*	9.96 ± 0.66*
SNP-B	25.41 ± 2.82***	21.83 ± 3.77**	21.68 ± 1.36***	31.08 ± 2.94***
SNP-C	55.52 ± 2.01***	13.37 ± 4.07*	17.91 ± 1.85***	13.21 ± 1.02**
		IMR90 cell lines		
untreated	99.79 ± 0.10	0.13 ± 0.04	0.08 ± 0.04	0.03 ± 0.01
standard drug	71.69 ± 1.66***	20.75 ± 1.48***	7.12 ± 0.13***	0.44 ± 0.05
SNP-B	97.08 ± 0.07	0.06 ± 0.03	0.49 ± 0.25	2.36 ± 0.30***
SNP-C	87.88 ± 3.83**	8.89 ± 3.54*	1.63 ± 0.50*	1.59 ± 0.29**

[a]Values are expressed as the mean ± SEM ($n = 3$). Statistical significance (P) calculated by one-way ANOVA followed by Dunnett's test. ***$P < 0.001$, **$P < 0.01$, and *$P < 0.05$ were considered as statistically significant by comparing the treated group with the control group.

https://doi.org/10.1021/acsomega.1c04047
ACS Omega 2021, 6, 32548−32562

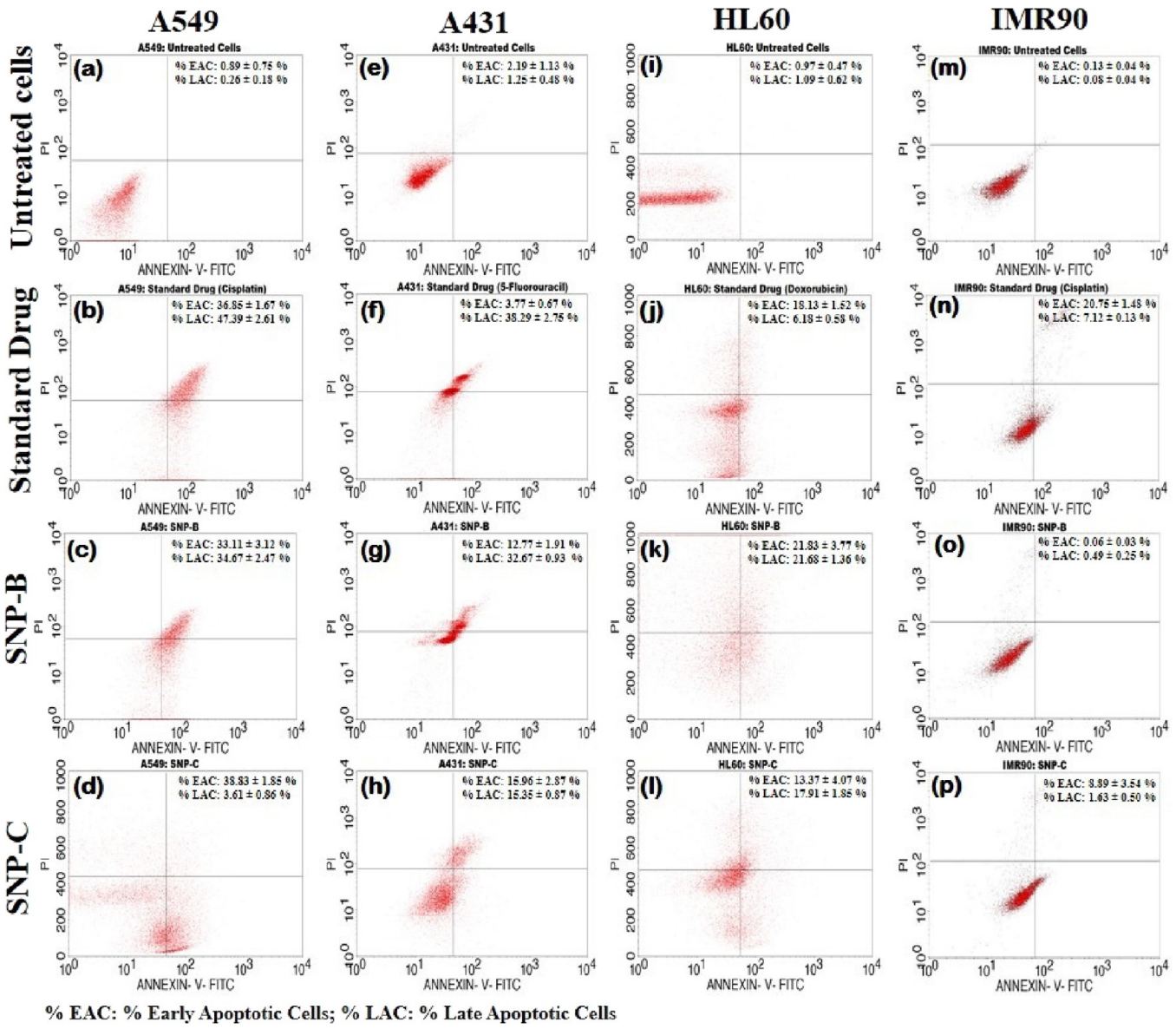

Figure 6. Apoptosis of A549, A431, HL60, and IMR90 cell-lines un-treated (a, e, i, m) and, treated with IC_{50} concentration of the standard drug (b, f, j, n), SNP-B (c, g, k, o), and SNP-C (d, h, l, p).

the cell lines treated with the standard drug and nano-sulfur showed an increased cell arrest compared to untreated cells. The percentage of cells arrested in the G2/M phase for SNP-B and SNP-C, respectively, was 39.31 ± 0.45 and 24.07 ± 0.77% for A549, 56.22 ± 1.60 and 28.05 ± 0.43% for A431, and 26.88 ± 0.41 and 45.31 ± 0.26% for HL60 cell lines. In contrast, the cell percentage in the G2/M phase of sulfur nanoparticle treated IMR90 cells was 40.43 ± 0.12% for SNP-B and 51.16 ± 0.26% for SNP-C. These results suggest that nano-sulfur inhibits the cellular proliferation via G_2/M phase cell cycle arrest. The extent of G_2/M phase cell cycle arrest was higher for SNP-B compared to SNP-C, indicating that SNP-B exhibits a higher cytotoxicity to the cell lines tested. The observed difference is concurrent with the cytotoxic results. In addition, an increase in sub-diploid peaks (sub G0/G1 phase) was observed for all the treated cancer cells when compared to untreated cells, reflecting the apoptotic population of cells.

Caspase-3 Expression Study. The molecular mechanism involved in induced apoptosis was investigated through caspase-3 antibody expression using flow cytometry. Expression levels of caspase-3 by A549, A431, HL60, and IMR90 cells exposed to nano-sulfur were compared with untreated cells. Results revealed a significant increase in the expression levels of caspase-3 in all the cell lines (A549, A431, HL60, and IMR90) treated with nano-sulfur compared to untreated cells (Table 4 and Figure 8). Exposure of A549 cells to SNP-B and SNP-C increased the mean fluorescence intensity (MFI) to 50.34 ± 1.13 and 37.98 ± 0.96, respectively, when compared to untreated cells (12.62 ± 0.69). The increase in MFI for A431 cell lines treated with SNP-B and SNP-C was 47.84 ± 0.47 and 26.16 ± 0.76, respectively, compared to untreated cells (9.59 ± 0.15). Similarly, for HL60 cell lines treated with SNP-B and SNP-C, MFI was 50.91 ± 2.71 and 39.36 ± 2.4, respectively, compared to untreated cells (8.63 ± 0.25), whereas a significant decrease in the mean fluorescence intensity of IMR90 cells treated with SNP-C and SNP-B was observed and found to be 21.25 ± 2.43 and 13.46 ± 1.36, respectively, in comparison with sulfur nanoparticle

https://doi.org/10.1021/acsomega.1c04047
ACS Omega 2021, 6, 32548−32562

Table 3. Cell Cycle Analysis of SNP-B and SNP-C against A549, A431 HL60, and IMR90 Cell Lines[a]

sl. no	cell cycle stage	untreated	standard drug	SNP-B	SNP-C
			A549 cell lines		
1	sub G0/G1	1.00 ± 0.13	3.17 ± 0.51**	3.49 ± 0.39**	3.39 ± 0.32**
2	G0/G1	79.41 ± 0.38	36.55 ± 0.39***	42.05 ± 0.59***	60.46 ± 0.73***
3	S	9.78 ± 0.61	11.27 ± 0.58	5.37 ± 0.49***	8.58 ± 0.29*
4	G2/M	9.81 ± 0.36	32.80 ± 1.27***	39.31 ± 0.45***	24.07 ± 0.77***
			A431 cell lines		
1	sub G0/G1	2.77 ± 0.14	17.36 ± 1.30***	4.9 ± 0.84	12.17 ± 0.19***
2	G0/G1	54.77 ± 0.71	30.46 ± 2.7***	21.7 ± 0.72***	29.71 ± 1.92***
3	S	19.46 ± 1.27	26.91 ± 1.35*	17.42 ± 1.07	29.87 ± 1.67**
4	G2/M	22.96 ± 0.78	25.1 ± 0.22	56.22 ± 1.60***	28.05 ± 0.43*
			HL60 cell lines		
1	sub G0/G1	7.8 ± 0.31	15.68 ± 1.58***	7.74 ± 0.7	3.76 ± 0.14*
2	G0/G1	56.12 ± 0.84	34.36 ± 0.81***	41.53 ± 1.01***	26.61 ± 0.9***
3	S	12.65 ± 0.76	21.76 ± 0.51***	22.53 ± 0.89***	20.83 ± 0.56***
4	G2/M	22.23 ± 0.07	25.74 ± 1.15*	26.88 ± 0.41**	45.31 ± 0.26***
			IMR90 cell lines		
1	sub G0/G1	0.89 ± 0.06	0.58 ± 0.12**	0.52 ± 0.05***	1.48 ± 0.02***
2	G0/G1	50.03 ± 0.13	34.62 ± 0.19***	49.09 ± 0.34	39.17 ± 1.54***
3	S	4.57 ± 0.17	9.13 ± 0.44***	5.18 ± 0.50	4.7 ± 0.35
4	G2/M	44.37 ± 0.21	52.66 ± 0.28***	40.43 ± 0.12***	51.16 ± 0.26***

[a]Values are expressed as the mean ± SEM (n = 3). Statistical significance (P) calculated by one-way ANOVA followed by Dunnett's test. ***P < 0.001, **P < 0.01, and *P < 0.05 were considered as statistically significant by comparing the treated group with the control group.

treated A549, A431, and HL60 cells. The significant increment in caspase-3 expression of the treated cancer cells indicate that the apoptosis induced by nano-sulfur is through a caspase-mediated pathway. Caspase-3 expression was higher for SNP-B treated cells when compared to SNP-C treated cells. The higher caspase expression in SNP-B treated cells indicates the higher apoptotic cell death induced by SNP-B compared to SNP-C.

DISCUSSIONS

The cell viability assay exhibited a dose-dependent cytotoxic effect of the prepared nano-sulfur (SNP-B and SNP-C). The cytotoxic effect for SNP-B was higher compared to that for SNP-C against all the tested cell lines. The observed difference in the cytotoxic effect of nano-sulfur could be attributed to the different reducing agents used during synthesis or the altered morphology of SNP-B (nanosheets) and SNP-C (nanoparticles). Graphene oxide (rGO) nanosheets synthesized using green (ascorbic acid) or chemical (hydrazine) reducing agents have shown altered morphology and diverse cytotoxicity effect on alveolar cells.[47] The difference in the biological response of rGO variants was attributed to morphological discrepancies arising from synthetic variations. Their findings concluded that the morphology of the nanomaterial arbitrate metabolic processes is essential for regulating standard cell function.[47]

Nanosheets, based on their structural difference with respect to nanoparticles, offer a larger surface to volume ratio for cell interaction. They also exhibit high polarized charges compared to nanoparticles. Studies have proved that cells can internalize nanosheets, resulting in a higher interaction between the substrate and cells.[48] Internalization and cellular distribution will have a direct impact on the cytotoxicity of the nanosheets.[30] In the present study, sulfur nanosheets have shown a higher cytotoxicity compared to sulfur nanoparticles. The present study proves the impact of morphology on the cytotoxicity of nano-sulfur.

The mechanism of cytotoxic action of nano-sulfur is still not clear. Previous reports have shown that copper is an essential cofactor and a key molecule in MEK/ERK pathway,[49] by acting as chelate and inhibiting the proliferation of A345 and MCF-7 cell lines via the MEK/ERK pathway along with slowing down the mitotic division in cancer cells.[50] The drug disulfiram (bis(diethylthiocarbamoyl)disulfide) was shown to exhibit specific anticancer activity due to the copper complexing ability of diethyldithiocarbamate, a reduced metabolite of disulfiram. The anticancer activity of the drug was mainly due to the interaction of copper(II) with the cellular protein complex resulting in the inhibition of proteasome function.[51] Tetrathiomolybdate, a sulfide releasing drug and a copper chelator, was shown to exhibit anti-angiogenic, anti-fibrogenic, and anti-inflammatory actions in preclinical studies.[52] Based on these reports, the cytotoxic activity of sulfur nanoparticles in the present study could be attributed to copper chelation and downregulation of protein expression responsible for mitosis. In addition to the above, morphological alterations such as cell clumping, irregular shape, rounding and detachment of cells from culture plates, cytoplasmic condensation, mitochondrial dysfunction, and loss of membrane integrity are also contributors for the cytotoxic activity of nano-sulfur.[53,54]

The event of a cell death is marked by the activation of specific cell signaling pathways characterized by different morphological features comprising two major modes: a metabolic pathway mediated programmed cell death called "apoptosis" and a nonregulated, accidental cell death caused by not so specific physiological stress inducers called "necrosis". Most of the currently used anticancer drugs exploit the apoptotic signaling pathways to trigger cancer cell death. Effective screening for potential therapeutic drugs thereby necessitates analysis of cell cycle progression and apoptotic-induced cell death. The cell cycle assay indicated that nano-sulfur inhibits cellular proliferation via a G2/M phase cell cycle arrest. An increase in sub-diploid peaks (sub G0/G1 phase) was observed for all the treated cells when compared to

https://doi.org/10.1021/acsomega.1c04047
ACS Omega 2021, 6, 32548−32562

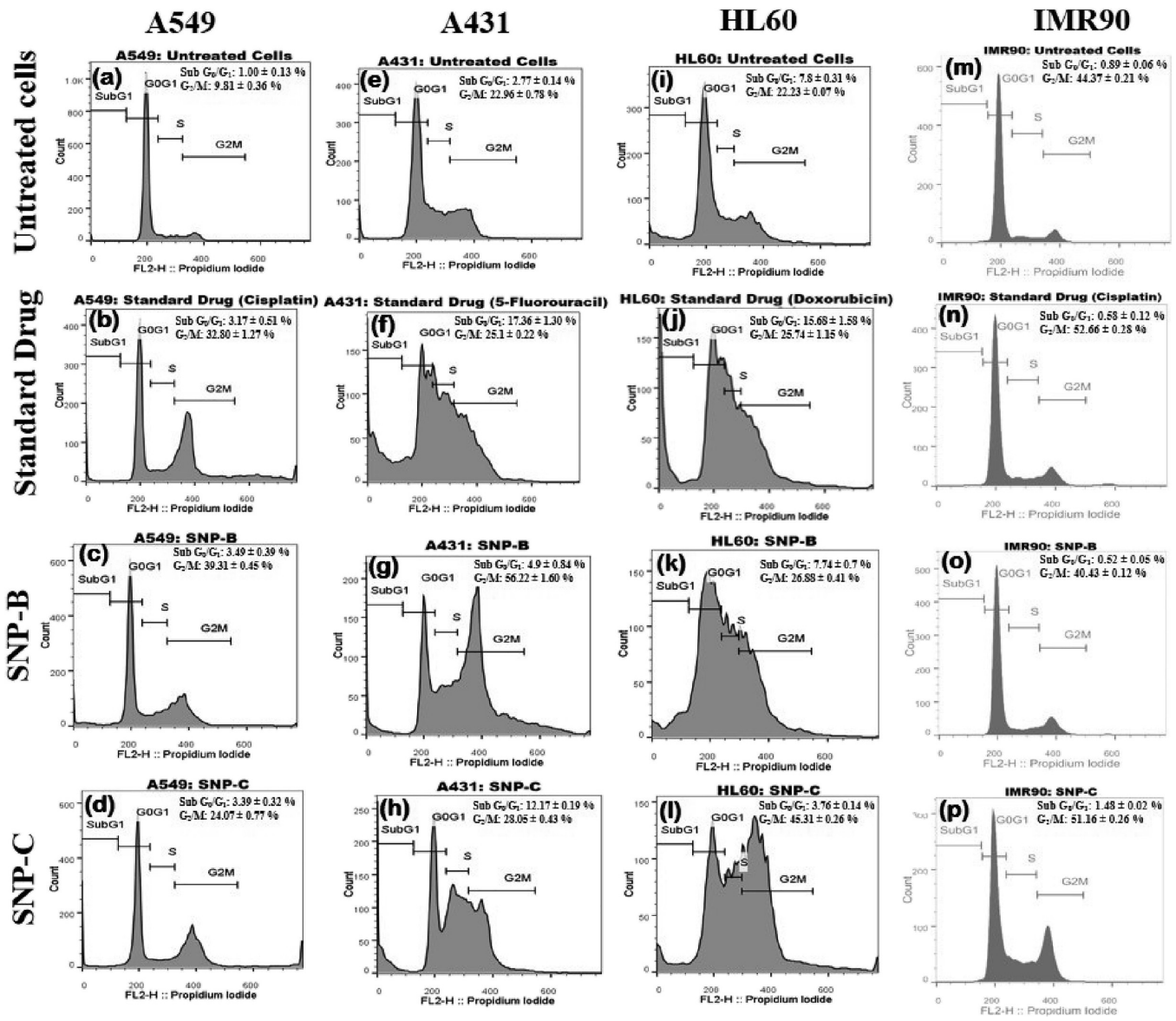

Figure 7. Cell cycle analysis of A549, A431, HL60, and IMR90 cell lines untreated (a, e, i, m) and, treated with IC_{50} concentration of the standard drug (b, f, j, n), SNP-B (c, g, k, o), and SNP-C (d, h, l, p).

Table 4. Caspase-3 Expression Study of SNP-B and SNP-C against A549, A431, HL60, and IMR90 Cell Lines[a]

	relative mean fluorescence intensity (MFI)			
sample	A549	A431	HL60	IMR90
untreated	12.62 ± 0.69	9.59 ± 0.15	8.63 ± 0.25	9.19 ± 0.92
standard drug	95.80 ± 0.57***	55.21 ± 0.45***	55.33 ± 2.3***	29.65 ± 2.03***
SNP-B	50.34 ± 1.13***	47.84 ± 0.47***	50.91 ± 2.71***	13.46 ± 1.36
SNP-C	37.98 ± 0.96***	26.16 ± 0.76***	39.36 ± 2.4***	21.25 ± 2.43**

[a]Values are expressed as the mean ± SEM (n = 3). Statistical significance (P) calculated by one-way ANOVA followed by Dunnett's test. ***P < 0.001, **P < 0.01, and *P < 0.05 were considered as statistically significant by comparing the treated group with the control group.

untreated cells, reflecting the apoptotic population of cells. The extent of G_2/M phase cell cycle arrest was higher for SNP-B compared to SNP-C, indicating that SNP-B exhibits higher cytotoxicity to the cell lines tested. Previous studies have shown enhanced cytotoxicity associated with increased cell cycle arrest.[55] The obtained results are in concurrence with the cytotoxic behavior observed for SNP-B and SNP-C. Sulfur and sulfur compounds are known to induce nuclear and chromatin condensation, cyclin B1 accumulation, phosphorylation of histone H3 at serine 10 (H3P), and DNA fragmentation resulting in the early impairment of cell proliferation.[56,57] Cell cycle arrest at a specific phase thereby inducing apoptosis is a common cytotoxic mechanism exhibited by anticancer drugs. Many studies have reported that nanoparticles arrest cell cycle at the G2/M phase with enhanced percentage of cells in the sub G0/G1 phase indicative of apoptotic cell death.[58,59]

https://doi.org/10.1021/acsomega.1c04047
ACS Omega 2021, 6, 32548−32562

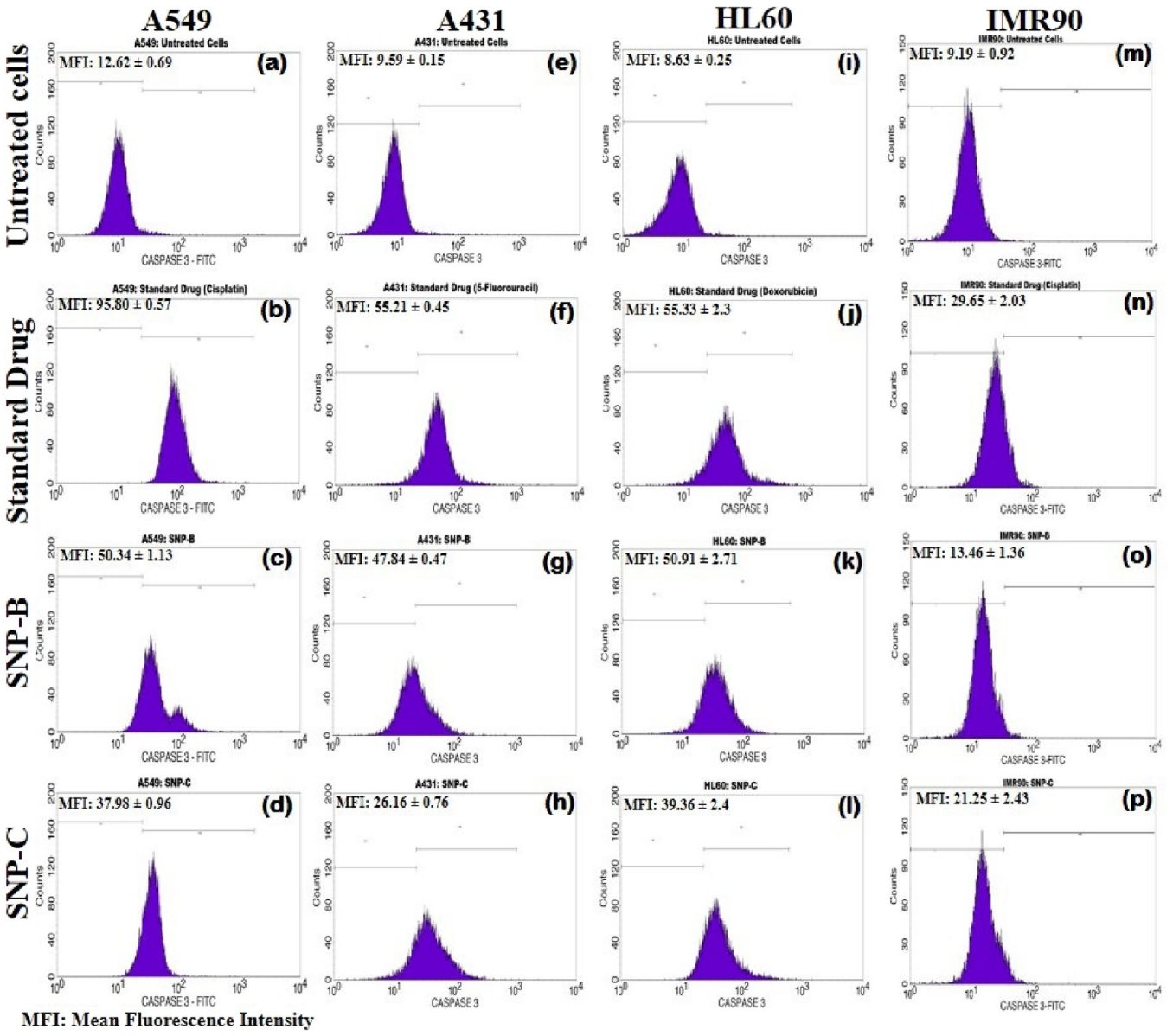

Figure 8. Caspase-3 expression of A549, A431, HL60, and IMR90 cell-lines un-treated (a, e, i, m), treated with IC_{50} concentration of the standard drug (b, f, j, n), SNP-B (c, g, k, o), and SNP-C (d, h, l, p).

The Annexin V−FITC/propidium iodide (PI) dual staining apoptotic assay indicated that nano-sulfur induces early cell apoptosis and late cell apoptosis indicative of apoptotic cell death in all the treated cell lines. Previous reports have shown that sulfur increases the expression of p53 protein, a multifunctional tumor suppressor that regulates apoptosis.[56] p53 increases the Bax expression and downregulates the Bcl-2 protein, resulting in the permeabilization of mitochondria, thus inducing apoptosis.[54,60,61] SNP-B exhibited higher apoptotic cell death in all the treated cell lines compared to SNP-C, considering both early and late apoptotic cell percentage. SNP-B is able to induce a higher rate of apoptotic activity even at its lower IC_{50} value compared to SNP-C, which is ineffectual to induce a comparable apoptotic activity even at its higher IC_{50} value. The obtained results clearly demonstrated the higher activity of sulfur nanosheets compared to sulfur nanoparticles.

The enhanced cytotoxic and apoptotic activity of the biogenic sulfur can be attributed to the many advantages of the 2D nanosheet morphology such as the large specific surface area for cell adhesion and internalization, abundance of sulfur atoms in ultrathin nanosheets, high capability of release of sulfur atoms, high polarized charges, and convenient attachment of different functional groups.[30,31] A study by Loutfy et al. on the cytotoxic effect of graphene oxide nanosheets toward HepG2 cancer cells has shown that the cytotoxic effect was due to the strong interaction with the phospholipid layer leading to internalization into mitochondria, nucleus, and cytoplasm, causing membrane integrity loss and damage.[62]

Further, SNP-B exhibited higher cytotoxic effects against cancer cell lines while showing minimum toxicity to normal cells compared to SNP-C. The difference in the cytotoxic effect of SNP-B toward normal and tumor cells could be due to the difference in the MEK/ERK pathway. Similar results have been reported by Shankar et al. in which nano-sulfur showed lower cytotoxicity to normal cell lines (CCD-986sk) compared to tumor cell lines (CT26).[15]

A distinctive feature of the early stages of apoptosis is the activation of caspase enzymes, which participate in the cleavage

https://doi.org/10.1021/acsomega.1c04047
ACS Omega 2021, 6, 32548−32562

of protein substrates and in the subsequent disassembly of the cell.[63] Cells treated with nano-sulfur had a significant increase in caspase-3 expression when compared to untreated cells. The higher apoptotic activity due to the significant expression of caspase-3 in case of nano-sulfur treated cells compared to untreated cells suggests that Bcl-2 protein clusters such as Bak and Bax were activated by p53 expression resulting in the formation of homo-oligomer leading to the release of cytochrome complex (Cytc) from the membrane interface. This would further lead to apoptosome formation and caspase-3 activation, thereby inducing mitochondrial intrinsic apoptosis.[64−66] Treatment with SNP-B resulted in a higher mean fluorescence intensity compared to SNP-C, indicating a higher expression of caspase-3 by SNP-B treated cells. The higher caspase expression in SNP-B treated cells indicates higher apoptotic cell death induced by SNP-B compared to SNP-C. Caspase-3 expression studies suggest that nano-sulfur was effective to activate mitochondrial mediated caspase dependent apoptosis on the treated cancer cell lines (A549, A431, and HL60).

Cancer therapy induced by apoptotic cell death alone without intrinsic cytotoxicity is likely to cause death of more normal cells than tumor cells. An effective cancer therapy requires drugs that are both cytotoxic and apoptotic. The synthesized biogenic sulfur nanosheets, with intrinsic cytotoxicity and apoptotic activity, can prove to be a potential chemopreventive drug.

CONCLUSIONS

The present study demonstrates the synthesis of nano-sulfur of varying morphologies using biological and chemical reducing agents. The *Punica granatum* peel extract as a reducing agent resulted in nanosheets of sulfur (SNP-B), while oxalic acid as a reducing agent produced aggregates of sulfur nanoparticles (SNP-C). Nano-sulfur synthesized nanoparticles were characterized using XRD, SEM, TEM, and Raman Spectroscopy. The *in vitro* anticancer activity of synthesized nanoparticles was evaluated against A549, A431, HL60, and IMR90 cell lines via a series of assays such as cell viability, apoptosis, cell cycle analysis, and caspase-3 studies. Biogenic nanoparticles (SNP-B) exhibited higher cytotoxicity in comparison to chemogenic nanoparticles (SNP-C) against all the tested cancer cell lines. In addition, significant apoptotic activity and G2/M phase of cell cycle arrest, and increased caspase-3 expression were observed in biogenic nanoparticles than chemogenic nanoparticles against A549, A431, and HL60 cell lines, indicating cancer cell death via the intrinsic apoptotic pathway mediated by mitochondria. Apart from this, the lower cytotoxicity observed in IMR90 cell lines treated with SNP-B compared to SNP-C indicated higher specificity of synthesized nanoparticles toward cancer cells. In conclusion, the study demonstrated morphology-dependent cytotoxic and apoptotic properties of nano-sulfur. Biogenic sulfur nanosheets, with intrinsic cytotoxicity and apoptotic activity, can prove to be a potential chemopreventive drug.

MATERIALS AND METHODS

Materials. Sodium thiosulfate pentahydrate ($Na_2S_2O_3 \cdot 5H_2O$; 99.5%), oxalic acid dihydrate ($(COOH)_2 \cdot 2H_2O$, 99.5%), and cetyltrimethyl ammonium bromide (CTAB, $C_{19}H_{42}BrN$, 99%) were obtained from Sisco Research Laboratories Pvt. Ltd., India. The details of other chemicals and material used in this study are as follows; Cell culture medium, (DMEM high glucose medium) (#AL111, HiMedia Laboratories Pvt. Ltd., India), fetal bovine serum (#RM10432, HiMedia), MTT reagent ($C_{18}H_{16}BrN_5S$; #4060 HiMedia, 5 mg/mL), cisplatin ($Pt(NH_3)_2Cl_2$, 99.9%; trade name: Platinol and Platinol-AQ-#PHR 1624 Sigma-Aldrich Pvt. Ltd., India), 5-fluorouracil ($C_4H_3FN_2O_2$, 99.9%; #F6627 Sigma-Aldrich Pvt. Ltd., India), doxorubicin hydrochloride ($C_{27}H_{29}NO_{11}$−≥98%; #324380 Sigma-Aldrich), apoptosis detection kit (cat. no.: 556547, Becton Dickinson (BD) Biosciences India Pvt. Ltd., India), cell cycle analysis kit (cat. no.: 550825, BD Biosciences), and caspase-3 assay kit (cat. no.: 560901, BD Biosciences). In addition, all the solutions and aqueous extract were prepared using double-distilled water.

Methods. *Preparation of the Aqueous Extract of Pomegranate Peel.* Peels of pomegranate (*Punica granatum*) fruits were washed thoroughly with distilled water to clean the dirt and debris. The clean peels were dried overnight at 50 °C in a hot air oven and powdered using a domestic mixer.Ten grams of the pomegranate peel powder was mixed with 100 mL of double-distilled water and heated for 45 min at 60 °C. The refluxed mixture resulted in a dark brown extract that was cooled to room temperature and centrifuged at 10,000 rpm for 10 min. The supernatant was collected and stored for further use.[67]

Synthesis of Chemogenic and Biogenic Nano-sulfur. Chemogenic nano-sulfur (SNP-C) was synthesized by the surfactant assisted acid catalyzed precipitation method.[19] Sodium thiosulfate pentahydrate (0.1 M), 0.1 M oxalic acid, and 0.05 M cetyltrimethylammonium bromide (CTAB) were used as precursor, weak acid, and surfactant, respectively. Oxalic acid and CTAB solutions were simultaneously added dropwise with continuous stirring to sodium thiosulfate solution. An equilibrium time of 40 min was allowed for completion of the reaction, resulting in precipitate formation. Sodium thiosulfate undergoes disproportionation reaction with the acidic solution to form sulfur and sulfonic acid according to reactions 1 and 2.[68]

$$Na_2S_2O_3 + 2H^+ \rightarrow 2Na^+ + SO_2 + S \downarrow + H_2O \quad (1)$$

$$SO_2 + H_2O \rightarrow H_2SO_3 \quad (2)$$

The obtained precipitate was sonicated at room temperature for 5 min in a bath sonicator, repeatedly washed with double-distilled water several times, and centrifuged for 10 min at 10,000 rpm. The obtained yellow precipitate was dried at 80 °C overnight.

For the biogenic synthesis of nano-sulfur (SNP-B), sodium thiosulfate pentahydrate ($Na_2S_2O_3 \cdot 5H_2O$, 1.24 g) was dissolved in 50 mL of pomegranate peel extract (PPE) under constant stirring for 10 min at room temperature and diluted to 100 mL with double-distilled water. To the above reaction mixture, oxalic acid solution [$(COOH)_2 \cdot 2H_2O$, 0.63 g] was added dropwise under constant stirring till a brownish white color solution was formed. The reaction mixture was allowed to equilibrate for 40 min that resulted in the formation of precipitate. The precipitate obtained was sonicated at room temperature for 5 min using a bath sonicator, repeatedly washed with double-distilled water, and centrifuged for 10 min at 10,000 rpm. The obtained brownish yellow precipitate was dried overnight at 80 °C, which resulted in the yellow sulfur nanopowder.

https://doi.org/10.1021/acsomega.1c04047
ACS Omega 2021, 6, 32548−32562

Characterization Studies. Synthesized nano-sulfur (SNP-C and SNP-B) was characterized using various analytical techniques. Powder X-ray diffraction analysis to confirm the crystalline phases of samples (PXRD) was carried out using Rigaku Ultima IV, Japan, with Cu K_α radiation (λ = 1.541 Å) equipped with nickel filters. Analysis of morphology, structure, and size of samples was carried out using scanning electron microscopy (SEM, Carl Zeiss- ULTRA 55, Germany) and high-resolution transmission electron microscopy (HRTEM, Jeol/JEM 2100, 200 kV, LaB6 filament). Raman spectroscopy (Jobin Yvon iHR550, Japan) was carried out to analyze the chemical structure of the samples.

Reviving of Cell Lines and Maintenance of Cell Culture. Human epidermoid carcinoma (A431), human promyelocytic leukemia (HL60) ,human lung carcinoma (A549), and human lung fibroblast (IMR90) cell lines were procured from the National Centre for Cell Science (NCCS), Pune, India. The cell lines were cultured using Dulbecco's modified Eagle's medium (DMEM) supplemented with 100 μg/mL streptomycin, 100 U/mL penicillin, and 5% (v/v) fetal bovine serum in a 5% CO_2 incubator at 37 °C and subcultured for every 3−4 days.

In Vitro Cytotoxic Studies. Cytotoxicity studies such as the cell viability assay and apoptosis, cell cycle, and caspase-3 studies were evaluated to assess the dose-dependent effect of synthesized nano-sulfur (SNP-C and SNP-B) against three different types of cell lines, viz., human lung carcinoma (A549), human epidermoid carcinoma (A431), human promyelocytic leukaemia (HL60), and human lung fibroblast cell lines (IMR90). Cisplatin (25 μM), 5-fluorouracil (12.5 μM), and doxorubicin (10 μM) were used as standard drug against A549 and IMR90, A431, and HL60 cell lines, respectively. Untreated cells were used as control.

Cell Viability Assay. An MTT (3-(4,5-dimethylthiazol-2-yl)-2,5-diphenyl tetrazolium bromide) assay was used to assess the viability of cells treated with sodium thiosulfate (ST), pomegranate peel extract (PPE), and nano-sulfur, respectively. A total of 2 × 10^4 cells/mL of A549, A431, HL60, and IMR90 cell lines were seeded in 96-well plates and incubated for 24 h at 37 °C. Once confluence was reached, cells were exposed to various concentrations (12.5, 25, 50, 100, and 200 μg/mL) of sodium thiosulfate (ST), pomegranate peel extract (PPE), and nano-sulfur (SNP-C and SNP-B) and incubated in CO_2 incubator (5%) for further 24 h at 37 °C. Post incubation, the spent medium was removed and cells were incubated with 100 μL of the MTT reagent (5 mg/mL) for 4 h. Excess MTT was removed after 4 h incubation, and formazan crystals were dissolved using 100 μL of DMSO. Gentle stirring was carried out using a gyratory shaker to enhance the dissolution. The viability of cells was measured on a microplate reader at an absorbance wavelength of 570 nm using the reference standard at 630 nm.[60] Further, a linear regression equation was used to determine the IC_{50} value and percentage cell viability.[69]

Analysis of Apoptotic Activity. To study apoptosis, 3 × 10^5 cells per well (A549, A431, and HL60) were seeded in six-well plates and incubated for 24 h at 37 °C. Cells were treated with IC_{50} concentration of SNP-C (A549: 9.53 ± 0.29 μg/mL, A431: 18.29 ± 0.09 μg/mL, HL60: 10.49 ± 0.52 μg/mL, and IMR90: 342.7 ± 12.29 μg/mL) and SNP-B (A549: 129.3 ± 0.23 μg/mL, A431: 122.4 ± 1.69 μg/mL, HL60: 153.2 ± 0.19 μg/mL, and IMR90: 443.8 ± 5.11 μg/mL), respectively, and incubated for 24 h at 37 °C in a CO_2 incubator (5%). Post incubation, floating and adherent cells were collected by a trypsinization procedure using 500 μL of the trypsin-EDTA solution (0.25% w/v). Cells were then harvested by centrifugation at 1800 rpm by washing with 1× PBS for 5 min. The obtained pellet was stained with 5 μL of AnnexinV−fluorescein isothiocyanate (FITC) for 15 min at room temperature in the dark followed by sequential addition of a binding buffer (400 μL) and 10 μL of propidium iodide (PI). Samples were then analyzed using a Becton Dickinson FACSCalibur flow cytometer. Each sample analysis was carried out by counting the effect on 10,000 cells.[70]

Cell Cycle Analysis by Flow Cytometry. Analysis of cell cycle arrest was carried out using six-well plates in which 2 × 10^5 cells per well (A549, A431, HL60, and IMR90) were seeded and exposed to IC_{50} concentration of SNP-C and SNP-B, respectively. The plates were incubated at 37 °C for 24 h in a CO_2 incubator (5%). Post incubation, adherent cells and floating cells were collected and washed with 1× PBS. Cell fixation was carried out using 70% cold ethanol. Cells were further suspended in PBS, and 400 μL of propidium iodide (PI) and 50 μL of the RNaseA solution were added. Well plates containing test compounds and untreated cells were incubated for 10 to 15 min at room temperature. Flow cytometry was carried out using a FACSCalibur flow cytometer for sample sets of 10,000 cells.[71]

Caspase-3 Expression Study. Caspase-3 activity was determined by using a caspase-3 assay kit. A549, A431, HL60, and IMR90 cells were seeded in six-well plates (3 × 10^5cells per well) and treated with IC_{50} concentration of SNP-C and SNP-B, respectively. The plates were incubated at 37 °C for 24 h in a CO_2 incubator (5%). Post incubation, cells were trypsinized using 500 μL of the trypsin-EDTA solution (0.25% w/v) and harvested by centrifuging at 1800 rpm for 5 min. Cells were fixed by prechilled 70% ethanol and washed with 1× PBS. Following washing with PBS, 5 μL of the FITC caspase-3 antibody was added, incubated for 30 min at room temperature in dark, and washed with 1× PBS containing 0.1% w/v sodium azide. Samples were analyzed using a flow cytometer for sample sets of 10,000 cells.[63]

Statistical Analysis. All the experiments were carried out in triplicate (n = 3), and the results are presented as mean ± SEM. The statistical significance (P) of differences between values was determined by one-way ANOVA using the ezANOVA (Version 0.985) software. P values ≤0.05 and ≤0.01 were considered as statistically significant.

■ ASSOCIATED CONTENT

Supporting Information

The Supporting Information is available free of charge at https://pubs.acs.org/doi/10.1021/acsomega.1c04047.

Cytotoxicity analysis of sodium thiosulfate (ST) and pomegranate peel extract (PPE) samples carried out via the MTT assay (Table S1 and Figure S1) (PDF)

■ AUTHOR INFORMATION

Corresponding Authors

Chandraprabha M. Naganna − *Department of Biotechnology, M.S. Ramaiah Institute of Technology (Affiliated to Visvesvaraya Technological University, Belgaum), Bangalore, Karnataka 560 054, India*; Email: chandraprabhamn@yahoo.com

Hari Krishna Rajan − *Department of Chemistry, M.S. Ramaiah Institute of Technology, Bangalore, Karnataka 560*

https://doi.org/10.1021/acsomega.1c04047
ACS Omega 2021, 6, 32548−32562

054, India; orcid.org/0000-0003-4939-2781; Email: rhk.chem@gmail.com

Authors

Samrat Krishnappa − *Department of Biotechnology, M.S. Ramaiah Institute of Technology (Affiliated to Visvesvaraya Technological University, Belgaum), Bangalore, Karnataka 560 054, India*

Sharath Rajashekarappa − *Department of Food Technology, Davangere University, Davanagere, Karnataka 577002, India*

Harish Basavanthappa Gowdru − *Department of MCA, UBDT College of Engineering, Davanagere, Karnataka 577004, India*

Complete contact information is available at: https://pubs.acs.org/10.1021/acsomega.1c04047

Notes

The authors declare no competing financial interest.

■ ACKNOWLEDGMENTS

We would like to express our deepest regards for DST-SAIF, KOCHI, India, and the Indian Institute of Science, Bangalore, India, for their support and help toward characterization analysis.

■ ABBREVIATION

ST	sodium thiosulfate
PPE	pomegranate peel extract
SNP-C	chemogenic nano-sulfur
SNP-B	biogenic nano-sulfur
PPE	pomegranate peel extract
CTAB	cetyltrimethyl ammonium bromide
MTT	3-(4,5-dimethylthiazol-2-yl)-2,5-diphenyl-tetrazolium bromide
A549	human lung carcinoma cell line
A431	human epidermoid carcinoma cell line
HL60	human promyelocytic leukemia cell line
DMEM	Dulbecco's modified Eagle's medium
Annexin V−FITC	AnnexinV−fluorescein isothiocyanate
PI	propidium iodide
IC_{50}	half-maximal inhibitory concentration
PXRD	powder X-ray diffraction
SEM	scanning electron microscopy
TEM	transmission electron microscopy
MAPK	mitogen activated protein kinase
ERK	extracellular activation kinase
MFI	mean fluorescence intensity
Cytc	cytochrome complex
p53	tumor suppressor protein

■ REFERENCES

(1) Sung, H.; Ferlay, J.; Siegel, R. L.; Laversanne, M.; Soerjomataram, I.; Jemal, A.; Bray, F. Global Cancer Statistics 2020: GLOBOCAN Estimates of Incidence and Mortality Worldwide for 36 Cancers in 185 Countries. *CA Cancer J Clin.* **2021**, 209−249.

(2) GLOBOCAN *2020: India Factsheet*; https://gco.iarc.fr/today/data/factsheets/populations/356-india-fact-sheets . pdf, 2021 (Accessed in 19 September 2021).

(3) Zheng, S.; Li, X.; Zhang, Y.; Xie, Q.; Wong, Y. S.; Zheng, W.; Chen, T. PEG-Nanolized Ultrasmall Selenium Nanoparticles Overcome Drug Resistance in Hepatocellular Carcinoma HepG2 Cells through Induction of Mitochondria Dysfunction. *Int. J. Nanomed.* **2012**, *7*, 3939−3949.

(4) Gao, Y.; Xie, J.; Chen, H.; Gu, S.; Zhao, R.; Shao, J.; Jia, L. Nanotechnology-Based Intelligent Drug Design for Cancer Metastasis Treatment. *Biotechnol. Adv.* **2014**, *32*, 761−777.

(5) Heath, J. R.; Davis, M. E. Nanotechnology and Cancer. *Annu. Rev. Med.* **2008**, *59*, 251−265.

(6) Rai, M.; Ingle, A. P.; Paralikar, P. Sulfur and Sulfur Nanoparticles as Potential Antimicrobials: from Traditional Medicine to Nanomedicine. *Expert Rev. Anti-infect. Ther.* **2016**, *14*, 969−978.

(7) Shankar, S.; Jaiswal, L.; Rhim, J.-W. New insight into Sulfur Nanoparticles: Synthesis and Applications. *Crit. Rev. Environ. Sci. Technol.* **2021**, *51*, 2329−2356.

(8) Jha, D. K.; Debata, L. A Case of Vitiligo Treated by Sulphur. *Int. J. Res. Homoe.* **2009**, *3*, 34−40.

(9) Lee, Z. W.; Zhou, J.; Chen, C. S.; Zhao, Y.; Tan, C. H.; Li, L.; Moore, P. K.; Deng, L. W. The Slow-Releasing Hydrogen Sulfide Donor, GYY4137, Exhibits Novel Anti-Cancer Effects *In Vitro* and *In Vivo*. *PLoS One* **2011**, *6*, No. e21077.

(10) Duan, F.; Li, Y.; Chen, L.; Zhou, X.; Chen, J.; Chen, H.; Li, R. Sulfur Inhibits the Growth of Androgen-Independent Prostate Cancer *In Vivo*. *Oncol. Lett.* **2015**, *9*, 437−441.

(11) Hedderich, R.; Klimmek, O.; Kroger, A.; Dirmeier, R.; Keller, M.; Stetter, K. O. Anaerobic Respiration with Elemental Sulfur and With Disulfides. *FEMS Microbiol. Rev.* **1998**, *22*, 353−381.

(12) Seh, Z. W.; Li, W.; Cha, J. J.; Zheng, G.; Yang, Y.; McDowell, M. T.; Hsu, P.-C.; Cui, Y. Sulfur−TiO_2Yolk−Shell Nanoarchitecture with Internal Void Space for Long-Cycle Lithium−Sulfur Batteries. *Nat. Commun.* **2013**, *4*, 1331.

(13) Thakur, S.; Das, G.; Raul, P. K.; Karak, N. Green One-Step Approach to Prepare Sulfur/Reduced Graphene Oxide Nanohybrid for Effective Mercury Ions Removal. *J. Phys. Chem. C* **2013**, *117*, 7636−7642.

(14) Islamov, R. A.; Bishimova, I.; Sabitov, A. N.; Ilin, A. I.; Burkitbaev, M. M. Lack of Mutagenic Activity of Sulfur Nanoparticles in Micronucleus Test on L5178Y Cell Culture. *Cell tissue biol.* **2018**, *12*, 27−32.

(15) Shankar, S.; Pangeni, R.; Park, J. W.; Rhim, J. W. Preparation of Sulfur Nanoparticles and their Antibacterial Activity and Cytotoxic Effect. *Mater. Sci. Eng. C.* **2018**, *92*, 508−517.

(16) Guo, Y.; Deng, Y.; Hui, Y.; Zhao, J.; Zhang, B. Synthesis and Characterization of Sulfur Nanoparticles by Liquid Phase Precipitation Method. *Acta Chim. Sin.* **2005**, *63*, 337−340.

(17) Guo, Y.; Zhao, J.; Yang, S.; Yu, K.; Wang, Z.; Zhang, H. Preparation and Characterization of Monoclinic Sulfur Nanoparticles by Water-in-Oil Microemulsions Technique. *Powder Technol.* **2006**, *162*, 83−86.

(18) Deshpande, A. S.; Khomane, B. R.; Vaidya, B. K.; Joshi, R. M.; Harle, A. S.; Kulkarni, B. D. Sulfur Nanoparticles Synthesis and Characterization from H_2S gas, using Novel Biodegradable Iron Chelates in w/o Microemulsion. *Nanoscale Res. Lett.* **2008**, *3*, 221−229.

(19) Chaudhuri, R. G.; Paria, S. Synthesis of Sulfur Nanoparticles in Aqueous Surfactant Solutions. *J. Colloid Interface Sci.* **2010**, *343*, 439−446.

(20) Salem, N. M.; Albanna, L. S.; Awwad, A. M.; Ibrahim, Q. M.; Abdeen, A. O. Green Synthesis of Nano-Sized Sulfur and its Effect on Plant Growth. *J. Agric. Sci.* **2015**, *8*, 188−194.

(21) Awwad, A. M.; Salem, N. M.; Abdeen, A. O. Noval Approach for Synthesis Sulfur (SNPs) Nanoparticles using *Albiziajulibrissin* Fruits Extract. *Adv. Mat. Lett.* **2015**, *6*, 432−435.

(22) Kouzegaran, V. J.; Farhadi, K. Green Synthesis of Sulfur Nanoparticles Assisted by aHerbal Surfactant in Aqueous Solutions. *Micro Nano Lett.* **2017**, *12*, 329−334.

(23) Tripathi, R. M.; Rao, R. P.; Tsuzuk, T. Green synthesis of sulfur nanoparticles and evaluation of their catalytic detoxification of hexavalent chromium in water. *RSC Adv.* **2018**, *8*, 36345.

(24) Khairan, K.; Zahraturriaz; Jalil, Z. Green Synthesis of Sulphur Nanoparticles using Aqueous Garlic Extract (Allium sativum). *Rasayan J. Chem.* **2019**, *12*, 50−57.

(25) Bankole, O. M.; Osuntokun, O. T.; Adeola, A.; Owoeye, A. *Ocimum gratissimum* Capped Sulfur Nanoparticles and Antibacterial Efficacy against Multidrug- Resistant Microbes. *Asian J. Res. Biochem.* **2020**, *7*, 84−95.
(26) Al Banna, L. S.; Salem, N. M.; Jaleel, G. A.; Awwad, A. M. Green Synthesis of Sulfur Nanoparticles using *Rosmarinus officinalis* Leaves Extract and Nematicidal Activity against *Meloidogyne javanica*. *Chem. Int.* **2020**, *6*, 137−143.
(27) Ragab, G. A.; Saad-Allah, K. M. Green Synthesis of Sulfur Nanoparticles using *Ocimum basilicum* Leaves and its Prospective Effect on Manganese-Stressed *Helianthus annuus* (L.) Seedlings. *Ecotox. Environ. Safe.* **2020**, *191*, 110242.
(28) Najafi, S.; Razavi, S. M.; Khoshkam, M.; Asadi, A. Effects of Green Synthesis of Sulfur Nanoparticles from *Cinnamomum zeylanicum* Barks on Physiological and Biochemical Factors of Lettuce (*Lactuca sativa*). *Physiol. Mol. Biol. Plants.* **2020**, *26*, 1055−1066.
(29) Priyadarshi, R.; Roy, S.; Rhim, J. W. Enhanced Functionality of Green Synthesized Sulfur Nanoparticles using Kiwifruit (*Actinidiadeliciosa*) Peel Polyphenols as Capping Agents. *J Nanostruct Chem.* **2021**, DOI: 10.1007/s40097-021-00422-9.
(30) Huang, W.; Sunami, Y.; Kimura, H.; Zhang, S. Applications of Nanosheets in Frontier Cellular Research. *Nanomaterials* **2018**, *8*, 519.
(31) Kumar, N.; George, B. P. A.; Abrahamse, H.; Parashar, V.; Ngila, J. C. Sustainable One-Step Synthesis of Hierarchical Microspheres of PEGylated Mo_{S2} Nanosheets and MoO_3 Nanorods: Their Cytotoxicity Towards Lung and Breast Cancer Cells. *Appl. Surf. Sci.* **2017**, *396*, 8−18.
(32) Debye, P.; Scherrer, P. Interferenzen an Regellos Orientierten Teilchen im Réntgenlicht. *Physik.* **1916**, *17*, 277−282.
(33) Singh, J.; Dutta, T.; Kim, K. H.; Rawat, M.; Samddar, P.; Kumar, P. Green Synthesis of Metals and their Oxide Nanoparticles: Applications for Environmental Remediation. *J. Nanobiotechnol.* **2018**, *16*, 1−24.
(34) Sekkina, M. A.; El-Shereafy, E. S.; Mashaly, A.; El-Ashry, M. γ-Pyrolysis of Crystalline Sodium Thiosulphate Pentahydrate. *J. Radioanal. Nucl. Chem.* **1998**, *237*, 113−119.
(35) Young, J. E.; Pan, Z.; Teh, H. E.; Menon, V.; Modereger, B.; Pesek, J. J.; Matyska, M. T.; Dao, L.; Takeoka, G. Phenolic Composition of Pomegranate Peel Extracts using an liquid chromatography−mass spectrometry Approach with Silica Hydride Columns. *J. Sep. Sci.* **2017**, *40*, 1449−1456.
(36) Akhtar, S.; Ismail, T.; Fraternale, D.; Sestili, P. Pomegranate peel and peel extracts: Chemistry and food features. *Food Chem.* **2015**, *174*, 417−425.
(37) Sukri, S. N. A. M.; Shameli, K.; Wong, M. M.-T.; Teow, S.-Y.; Chew, J.; Ismail, N. A. Cytotoxicity and Antibacterial Activities of Plant Mediated Synthesized Zinc Oxide (ZnO) Nanoparticles using *Punica granatum* (pomegranate) Fruit Peels Extract. *J. Mol. Struct.* **2019**, 118957−118965.
(38) Farrokhnia, M.; Karimi, S.; Askarian, S. Strong Hydrogen Bonding of Gallic Acid during Synthesis of an Efficient AgNPs Colorimetric Sensor for Melamine Detection via Dis-synthesis Strategy. *ACS Sustainable Chem. Eng.* **2019**, *7*, 6672−6684.
(39) Paralikar, P.; Rai, M. Bio-Inspired Synthesis of Sulfur Nanoparticles using Leaf Extract of Four Medicinal Plants with Special Reference to their Antibacterial Activity. *IET Nanobiotechnol.* **2017**, *12*, 25−31.
(40) Turcotte, S. B.; Benner, R. E.; Riley, A. M.; Li, J.; Wadsworth, M. E.; Bodily, D. Application of Raman Spectroscopy to Metal-Sulfide Surface Analysis. *Appl. Opt.* **1993**, *32*, 935−938.
(41) Guo, J.; Xu, Y.; Wang, C. Sulfur-Impregnated Disordered Carbon Nanotubes Cathode for Lithium−Sulfur Batteries. *Nano Lett.* **2011**, *11*, 4288−4294.
(42) Chen, F.; Yang, J.; Bai, T.; Long, B.; Zhou, X. Biomass Waste-Derived Honeycomb-Like Nitrogen and Oxygen Dual-Doped Porous Carbon for High Performance Lithium-Sulfur Batteries. *Electrochim. Acta* **2016**, *192*, 99−109.
(43) Wang, H.; Zhang, C.; Chen, Z.; Liu, H. K.; Guo, Z. Large-Scale Synthesis of Ordered Mesoporous Carbon Fiber and its Application as Cathode Material for Lithium−Sulfur Batteries. *Carbon* **2015**, *81*, 782−787.
(44) Scott, D. W.; McCullough, J. P.; Kruse, F. H. Vibrational Assignment and Force Constants of S_8 from A Normal-Coordinate Treatment. *J. Mol. Spectrosc.* **1964**, *13*, 313−320.
(45) Ward, A. T. Raman Spectroscopy of Sulfur, Sulfur-Selenium, and Sulfur-Arsenic Mixtures. *J. Phys. Chem.* **1968**, *72*, 4133−4139.
(46) Krętowski, R.; Kusaczuk, M.; Naumowicz, M.; Kotyńska, J.; Szynaka, B.; Cechowska-Pasko, M. The Effects of Silica Nanoparticles on Apoptosis and Autophagy of Glioblastoma Cell Lines. *Nanomaterials* **2017**, *7*, 230.
(47) Dervin, S.; Murphy, J.; Aviles, R.; Pillai, S. C.; Garvey, M. An *In Vitro* Cytotoxicity Assessment of Graphene Nanosheets on Alveolar Cells. *Appl. Surf. Sci.* **2018**, *434*, 1274−1284.
(48) Mendes, R. G.; Koch, B.; Bachmatiuk, A.; Ma, X.; Sanchez, S.; Damm, C.; Schmidt, O. G.; Gemming, T.; Eckert, J.; Rummeli, M. H. A Size Dependent Evaluation of the Cytotoxicity and Uptake of Nanographene Oxide. *J. Mater. Chem. B* **2015**, *3*, 2522−2529.
(49) Brady, D. C.; Crowe, M. S.; Turski, M. L.; Hobbs, G. A.; Yao, X.; Chaikuad, A.; Knapp, S.; Xiao, K.; Campbell, S. L.; Thiele, D. J.; Counter, C. M. Copper is Required for Oncogenic BRAF Signalling and Tumorigenesis. *Nature* **2014**, *509*, 492−496.
(50) Liu, H.; Zhang, Y.; Zheng, S.; Weng, Z.; Ma, J.; Li, Y.; Xie, X.; Zheng, W. Detention of Copper by Sulfur Nanoparticles Inhibits the Proliferation of A375 Malignant Melanoma and MCF-7 Breast Cancer Cells. *Biochem. Biophys. Res. Commun.* **2016**, *477*, 1031−1037.
(51) Skrott, Z.; Cvek, B. Diethyldithiocarbamate Complex with Copper: The Mechanism of Action in Cancer Cells. *Mini Rev. Med. Chem.* **2012**, *12*, 1184−1192.
(52) Medici, V.; Sturniolo, G. C. Tetrathiomolybdate, ACopper Chelator for the Treatment of Wilson Disease, Pulmonary Fibrosis and Other Indications. *IDrugs: Investig. Drugs. J.* **2008**, *11*, 592−606.
(53) Nirmala, J. G.; Akila, S.; Narendhirakannan, R. T.; Chatterjee, S. *Vitis vinifera* Peel Polyphenols Stabilized Gold Nanoparticles Induce Cytotoxicity and Apoptotic Cell Death in A431 Skin Cancer Cell Lines. *Adv. Powder Technol.* **2017**, *28*, 1170−1184.
(54) George, B. P. A.; Kumar, N.; Abrahamse, H.; Ray, S. S. Apoptotic Efficacy of Multifaceted Biosynthesized Silver Nanoparticles on Human Adenocarcinoma Cells. *Sci. Rep.* **2018**, *8*, 14368.
(55) Ling, Y. H.; El-Naggar, A. K.; Priebe, W.; Perez-Soler, R. Cell Cycle-Dependent Cytotoxicity, G2/M Phase Arrest, and Disruption of p34cdc2/cyclin B1 Activity Induced by Doxorubicin in Synchronized P388 Cells. *Mol. Pharmacol.* **1996**, *49*, 832−841.
(56) Lee, J.; Lee, H. J.; Park, J. D.; Lee, S. K.; Lee, S. I.; Lim, H. D.; Lee, Y. M.; Yun, Y. G.; Jeon, B. H.; Ree, I. S.; Jun, C. D.; Lee, S. K.; Kim, E. C. Anti-cancer Activity Of Highly Purified Sulfur in Immortalized and Malignant Human Oral Keratinocytes. *Toxicol. In Vitro* **2008**, *22*, 87−95.
(57) Wang, H.-C.; Yang, J.-H.; Hsieh, S.-C.; Sheen, L.-Y. Allyl Sulfides Inhibit Cell Growth of Skin Cancer Cells through Induction of DNA Damage Mediated G2/M Arrest and Apoptosis. *J. Agric. Food Chem.* **2010**, *58*, 7096−7103.
(58) Bendale, Y.; Bendale, V.; Paul, S. Evaluation of Cytotoxic Activity of Platinum Nanoparticles against Normal and Cancer Cells and its Anticancer Potential through Induction of Apoptosis. *Integr. Med. Res.* **2017**, *6*, 141−148.
(59) Namvar, F.; Rahman, H. S.; Mohamad, R.; Rasedee, A.; Yeap, S. K.; Chartrand, M. S.; Azizi, S.; Tahir, P. M. Apoptosis Induction in Human Leukemia Cell Lines by Gold Nanoparticles Synthesized Using the Green Biosynthetic Approach. *J. Nanomater.* **2015**, *2015*, 1.
(60) Foo, J. B.; Yazan, L. S.; Tor, Y. S.; Wibowo, A.; Ismail, N.; Armania, N.; Cheah, Y. K.; Abdullah, R. *Dillenia suffruticosa* Dichloromethane Root Extract Induced Apoptosis Towards MDA-MB-231Triple-Negative Breast Cancer Cells. *J. Ethnopharmacol.* **2016**, *187*, 195−204.
(61) A.T., Naito; I., Shiojima; I., Komuro, Novel *therapeutic targets and strategies against myocardial diseases, In Muscle: Fundamental*

Biology and Mechanisms of Disease; 1st ed., Hill, J. A.; Olson, E. N., Ed., Elsevier: San Diego, California 2012, pp. 739−744.
(62) Loutfy, S. A.; Salaheldin, T. A.; Ramadan, M. A.; Farroh, K. Y.; Abdallah, Z. F.; Youssef, T. Synthesis, Characterization and Cytotoxic Evaluation of Graphene Oxide Nanosheets: *In Vitro* Liver Cancer Model. *Asian Pac. J. Cancer Prev.* **2017**, *18*, 955−961.
(63) Kaplan, A.; Akalin Ciftci, G.; Kutlu, H. M. The Apoptotic and Genomic Studies on A549 Cell Line Induced by Silver Nitrate. *Tumor Biol.* **2017**, *39*, 1−12.
(64) Saha, S.; Bhattacharjee, P.; Guha, D.; Kajal, K.; Khan, P.; Chakraborty, S.; Mukherjee, S.; Paul, S.; Manchanda, R.; Khurana, A.; Nayak, D.; Chakrabarty, R.; Sa, G.; Das, T. Sulfur Alters NFκB-p300 Cross-Talk in Favour of p53-p300 to Induce Apoptosis in Non-Small Cell Lung Carcinoma. *Int. J. Oncol.* **2015**, *47*, 573−582.
(65) Adams, J. M.; Cory, S. Bcl-2 Regulated Apoptosis: Mechanism and Therapeutic Potential. *Curr. Opin. Immunol.* **2007**, *19*, 488−496.
(66) Zhang, J.; Huang, K.; O'Neill, K. L.; Pang, X.; Luo, X. Bax/Bak Activation in The Absence of Bid, Bim, Puma, and p53. *Cell Death Dis.* **2016**, *7*, No. e2266.
(67) Bharani, R. S. A.; Namasivayam, S. K. R. Biogenic Silver Nanoparticles Mediated Stress on Developmental Period and Gut Physiology of Major Lepidopteran Pest *Spodoptera litura* (Fab.) (Lepidoptera: Noctuidae)-An Eco-Friendly Approach of Insect Pest Control. *J. Environ. Chem. Eng.* **2017**, *5*, 453−467.
(68) Shankar, S.; Rhim, J. W. Preparation of Sulfur Nanoparticle-incorporated Antimicrobial Chitosan Films. *Food Hydrocolloids* **2018**, *82*, 116−123.
(69) Taherian, A.; Esfandiari, N.; Rouhani, S. Breast cancer drug delivery by novel drug-loaded chitosan-coated magnetic Open Access nanoparticles. *Cancer Nano.* **2021**, *12*, 15.
(70) Al-Zharani, M.; Nasr, F. A.; Alqahtani, A. S.; Cordero, M. A. W.; Alotaibi, A. A.; Bepari, A.; Alarifi, S.; Daoud, A.; Barnawi, I. O.; Daradka, H. M. *In Vitro* Cytotoxic Evaluation and Apoptotic Effects of *Datura innoxia* Grown in Saudi Arabia and Phytochemical Analysis. *Appl. Sci.* **2021**, *11*, 2864.
(71) Manzoor, S.; Bashir, D. J.; Imtiyaz, K.; Rizvi, M. M. A.; Ahamad, I.; Fatma, T.; Agarwal, N. B.; Arora, I.; Samim, M. Biofabricated Platinum Nanoparticles: Therapeutic Evaluation as a Potential Nanodrug against Breast Cancer Cells and Drug-Resistant Bacteria. *RSC Adv.* **2021**, *11*, 24900−24916.

https://doi.org/10.1021/acsomega.1c04047
ACS Omega 2021, 6, 32548−32562